Molecular Dynamics Simulations of Polyelectrolyte Solutions: Nonuniform Stretching of Chains and Scaling Behavior

Qi Liao,[†,‡] Andrey V. Dobrynin,[§] and Michael Rubinstein*[,†]

Department of Chemistry, University of North Carolina, Chapel Hill, North Carolina, 27599-3290; Polymer Physics and Chemistry Laboratory, Institute of Chemistry of the Chinese Academy of Sciences, Beijing 100080, P. R. China; and Polymer Program, Institute of Materials Science and Department of Physics, University of Connecticut, Storrs, Connecticut 06269-3136

Received December 20, 2002; Revised Manuscript Received March 3, 2003

ABSTRACT: We present the results of molecular dynamics simulations of polyelectrolyte solutions in near-Θ-solvent conditions for polymer backbone. Polyelectrolyte solutions are modeled as an ensemble of bead-spring chains of charged Lennard-Jones particles with explicit counterions. Simulations were performed for both fully and partially charged polyelectrolyte chains with the number of monomers N varying from 25 to 300 in the range of polymer concentrations covering both dilute and semidilute regime. Polyelectrolyte chains in dilute solutions are nonuniformly stretched with the projection of the linear monomer density onto the end-to-end vector increasing logarithmically from the middle of the chain. The simulation results for chain size dependence on the degree of polymerization at different polymer concentrations are in good qualitative agreement with predictions of the modified scaling model that takes into account nonuniform stretching of polyelectrolyte chains. In semidilute solutions we confirm that the correlation length is inversely proportional to the square root of polymer concentration. By measuring the bond angle correlation function, we have determined that polyelectrolyte chains can be viewed as flexible chains with the persistence length proportional to the correlation length. Our results for the concentration dependence of chain size R_e on polymer concentration for the longest chains (N = 187 and N = 300) are approaching the power law $c^{-1/4}$, predicted by the scaling model of salt-free polyelectrolyte solutions.

1. Introduction

Polyelectrolytes are polymers with ionizable groups.[1−8] In polar solvents such as water, these groups can dissociate, leaving charges on polymer chains and releasing counterions in solution. Electrostatic interactions between charges lead to the rich behavior of polyelectrolyte solutions qualitatively different from those of uncharged polymers.[9−11]

Computer simulations of polyelectrolytes over the past 20 years have proven to be a valuable tool for elucidation of structural and physical properties of charged systems as well as for verification of old models and creation of new theoretical models. The conformational properties of an isolated polyelectrolyte chain in a salt-free solution have been investigated by lattice Monte Carlo simulations[12−15] as well as by off-lattice Monte Carlo simulations of several different polyelectrolyte models: of a chain made of hard spheres connected by rigid bonds with fixed valence angles,[16] of a freely jointed chain,[17] and of a bead-spring chain.[18−22] These simulations support the scaling prediction that a polyelectrolyte chain crosses over from a coil to a rodlike (or extended) conformation with increasing strength of electrostatic interactions.

Systematic Monte Carlo (MC) studies of the polyelectrolyte size dependence on its degree of polymerization, performed by different groups,[18−22] have shown that the chain size grows with the degree of polymerization N as $R \sim N(\ln N)^{0.33}$. The nature of this deviation from the simple scaling law, $R \sim N$, is due to the variation of the elongation along the chain. Polyelectrolytes are more strongly stretched in the middle than at the ends, which yields a weak logarithmic correction to the chain size.[22,23]

With the explosive growth of computer power in recent years, it is possible to perform large-scale simulations of charged polymeric systems with explicit counterions.[24−29] Chemical details of real monomers are ignored in these simulations. Polyelectrolyte chains are modeled as connected monomers, with each monomer representing a group of chemical units. Solvent is modeled by a continuous medium, with macroscopic physical properties. In molecular dynamics simulations with explicit counterions, the long-range electrostatic interactions between charged species are taken into account by the Ewald summation method, including interactions with all periodic images of the system.

Recently, Stevens and Kremer[24−26] reported molecular dynamics simulations (MD) of dilute and semidilute polyelectrolyte solutions using spherical approximation of Adams and Dubey[30] for the Ewald sum. They found two regimes in the concentration dependence of the peak position in the monomeric structure factor. At low concentrations, the wavevector at the peak position scales with polymer concentration as $c^{1/3}$, which corresponds to the interchain correlations in dilute solutions. At higher concentrations the wavevector at the peak position scales is $c^{1/2}$ and corresponds to the correlation length in semidilute solutions.

Despite significant computational efforts, the puzzle of polyelectrolyte solutions is far from being completely resolved even for salt-free solutions. There are still some doubts about the validity of simple scaling assumptions

† University of North Carolina.
‡ Institute of Chemistry of the Chinese Academy of Sciences.
§ University of Connecticut.
* Corresponding author.

10.1021/ma025995f CCC: $25.00
Published on Web 04/10/2003

Table 1. Simulation Parameters

N	25	25	40	40	60	61	94	94	130	187	187	300
M	40	40	20	16	16	20	16	16	16	10	10	15
f	1	$^1/_3$	1	$^1/_3$	1	$^1/_3$	1	$^1/_3$	1	1	$^1/_3$	1

for strongly charged polyelectrolytes in the presence of counterion condensation. An unexpected result observed in simulations[26] was that the chains contract significantly due to counterion condensation before they actually overlap. It was argued that the fraction of condensed counterions increases with polymer concentration, leading to the decrease of the effective charge on the chain and resulting in contraction of polyelectrolyte chains even in dilute solutions. This effect of the counterion-mediated chain contraction was ignored in the simple scaling model (see ref 2 for review). Furthermore, these simulations did not support the correlation blobs' picture of semidilute polyelectrolyte solutions used in the scaling theories. The exponent for the concentration dependence of the chain size was reported in ref 26 to have much smaller absolute value than $^1/_4$ predicted by the scaling theory. This discrepancy can be attributed to the finite size effects in simulations of short chains. The simulations of solutions with longer polymers help illuminate the influence of chain ends on polyelectrolyte conformations. We performed molecular dynamics simulations of dilute and semidilute polyelectrolyte solutions aimed at elucidating the factors responsible for the discrepancy between the simple scaling predictions and the results of previous computer simulations.[24−26]

The rest of the manuscript is organized as follows. The simulation model and the algorithms are described in section 2. Section 3 gives a detailed account of the simulation results for the end-to-end distance, overlap concentration, correlation length, and the persistence length of polyelectrolytes in salt-free solutions as functions of chain length and polymer concentration. Finally, in section 4 we discuss our results.

2. Model and Methodology

Polyelectrolyte solution is represented by an ensemble of M bead-spring chains of N monomers, N_c counterions per chain, and fraction of charged monomers $f = N_c/N$ confined into a cubic simulation box of size L_c with periodic boundary conditions. All charged particles are taken to be monovalent ions, and therefore, the total number of charged monomers is equal to the number of counterions MN_c (see Table 1 for the values of these parameters). Excluded-volume interactions between every pair of monomers are included via the truncated Lennard-Jones (LJ) potential set to zero at the cutoff

$$U_{LJ}(r) = \begin{cases} 4\epsilon_{LJ}\left[\left(\frac{\sigma}{r}\right)^{12} - \left(\frac{\sigma}{r}\right)^{6} - \left(\frac{\sigma}{r_c}\right)^{12} + \left(\frac{\sigma}{r_c}\right)^{6}\right] & r \le r_c \\ 0 & r > r_c \end{cases} \quad (1)$$

where the cutoff distance is equal to $r_c = 2.5\sigma$. The parameter ϵ_{LJ} controls the strength of the short-range interactions, and the effective interaction parameter for the Θ condition is given by $(0.34 \pm 0.02)k_BT$ for the uncharged system.[27] Here, k_B is the Boltzmann constant and T is the absolute temperature. In all of our simulations we set ϵ_{LJ} to a value of $0.5k_BT$, which for strongly charged chains corresponds to a near-Θ condition, with thermal blob much larger than electrostatic blob.

The connectivity of monomers in the chains is maintained by the finite extension nonlinear elastic (FENE) potential

$$U_{FENE}(r) = -\frac{1}{2}kR_0^2 \ln\left(1 - \frac{r^2}{R_0^2}\right) \quad (2)$$

where $k = 7\epsilon_{LJ}/\sigma^2$ is the spring constant and $R_0 = 2\sigma$ is the maximum bond length at which the elastic energy of the bond becomes infinite. The FENE potential only gives the attractive part of the bond potential. The repulsive part of the bond potential is provided by the LJ interaction (eq 1).

A shifted Lennard-Jones potential is also used to describe the pure repulsive excluded-volume interactions between any pair of counterions and between a monomer and a counterion.

$$U_{LJ}^{S}(r) = \begin{cases} 4\epsilon_{LJ}\left[\left(\frac{\sigma}{r}\right)^{12} - \left(\frac{\sigma}{r}\right)^{6}\right] + \epsilon_{LJ} & r \le 2^{1/6}\sigma \\ 0 & r > 2^{1/6}\sigma \end{cases} \quad (3)$$

The parameter σ was chosen to be the same for both monomers and counterions.

Solvent molecules are not included explicitly in the simulations. The solvent is modeled by a dielectric medium with the dielectric constant ϵ. In such continuous representation of the solvent, all charged particles interact with each other via unscreened Coulomb potential

$$U_{Coul}(r) = k_BT\frac{l_Bq_iq_j}{r} \quad (4)$$

where q_i is the charge valence of the ith particle being equal to ± 1 for monovalent charges. The Bjerrum length $l_B = e^2/(\epsilon k_BT)$ determines the strength of the electrostatic interactions. In our simulations its value was chosen to be equal to 3σ. The electrostatic interactions between all charges in the simulation box and all of their periodic images were computed by the smoothed particle mesh Ewald (SPME) algorithm[31] implemented in the DL_POLY version 2.12 software package.[32]

We performed simulations of two different polyelectrolyte systems: (i) fully charged polyelectrolytes, with every monomer charged, and (ii) partially charged polyelectrolytes, with every third monomer carrying a charge.

The constant temperature ensemble simulations were performed by coupling system to the Langevin thermostat.[33] In this approach the motion of each particle is described by the Langevin equation

$$m\frac{d\vec{v}_i}{dt} = \vec{F}_i^R(t) - \beta\vec{v}_i + \vec{F}_i(t) \quad (5)$$

where $\vec{v}_i$ is velocity of the ith particle, m is the particle mass, $\vec{F}_i^R(t)$ is the stochastic force acting on the ith particle with zero average $\langle\vec{F}_i^R(t)\rangle = 0$, and delta-functional correlations $\langle F_{\alpha,i}^R(t)F_{\lambda,j}^R(t')\rangle = 2k_BT\beta\delta_\alpha\lambda\delta_{ij}\delta(t - t')$. $\vec{F}_i(t)$ is the net deterministic force from all other particles, which includes the contributions from the Lennard-Jones, FENE, and Coulomb terms described above, and β is the friction coefficient. The friction coefficient was set to $\beta = m/\tau_{LJ}$, where τ_{LJ} is the standard LJ time $\tau_{LJ} = (m\sigma/\epsilon_{LJ})^{1/2}$. The value of the friction coefficient β is $(k_BTm/2\sigma)^{1/2}$ because we set

$\epsilon_{LJ} = k_B T/2$ in our simulations. A velocity Verlet algorithm was used to integrate the equation of motion (eq 5) with a time step equal to $\Delta t = 0.014\tau_{LJ}$.

An alternative method was used to simulate a system of 15 chains with 300 beads coupled to the Nose-Hoover thermostat.[34] The Nose-Hoover thermostat is implemented by adding a time-dependent friction term to the Newton's equation of motion of the ith particle

$$\frac{d\vec{v}_i}{dt} = \frac{\vec{F}_i(t)}{m} - \chi\vec{v}_i \tag{6}$$

The friction coefficient χ is controlled by the first-order differential equation

$$\frac{d\chi}{dt} = \frac{1}{\tau_{NH}}\left(\frac{T}{T_{ext}} - 1\right) \tag{7}$$

where τ_{NH} is the time constant, which is equal to $0.5\tau_{LJ}$ in our simulations, T is the instantaneous temperature of the system, and T_{ext} is the temperature of the thermostat. This method appears to be more efficient than using the Langevin thermostat, leading to shorter relaxation time of the measurable chain properties, such as correlation function of the end-to-end vector.

We compared the results of simulations for the fully charged polyelectrolyte chains with the degree of polymerization $N = 94$ obtained by molecular dynamics simulations using the Langevin thermostat with those obtained from the simulations using the Nose-Hoover thermostat in both dilute ($c = 1.5 \times 10^{-3}\sigma^{-3}$) and semidilute ($c = 3.0 \times 10^{-3}\sigma^{-3}$) solutions. The polymer concentration c is defined as the number of monomers per unit volume. The results of both simulations are shown in Figure 1. As one can see, both methods give similar results for the chain size R_e (see Figure 1a) and the monomer−monomer pair correlation function $g(r)$ defined in eqs 27, 28, and 15 (see Figure 1b). However, the time correlation functions of end-to-end vectors, shown in Figure 1c for the same polyelectrolyte chains, decay almost 10 times faster for the Nose-Hoover thermostats in comparison with the Langevin thermostat.

The MD simulations were performed by the following procedure. The initial conformations of polyelectrolyte chains in the cubic cell with periodic boundary conditions were generated as a set of self-avoiding walks. The counterions were placed randomly in the free volume of the simulation box. The box contained between 15 and 40 chains in our simulations. Both dilute and semidilute solutions of chains with degree of polymerization N varying from 25 to 300 (see Table 1 for details), value of the Bjerrum length $l_B = 3\sigma$, were studied in the range of polymer concentrations c from $1.5 \times 10^{-7}\sigma^{-3}$ to $0.15\sigma^{-3}$. The simulations were carried out at constant temperature $T = 2\epsilon_{LJ}/k_B$ using the Langevin (for N between 25 and 187) or the Nose-Hoover thermostats (for $N = 300$). The number of MD steps was chosen large enough to allow the mean-square end-to-end distance and the mean-square radius of gyration to relax to their equilibrium values. This requirement led to the range of simulation runs between 100 000 and 4 000 000 MD steps (2−10 relaxation times of the end-to-end vector of chains) depending on the chain length and polymer concentration.

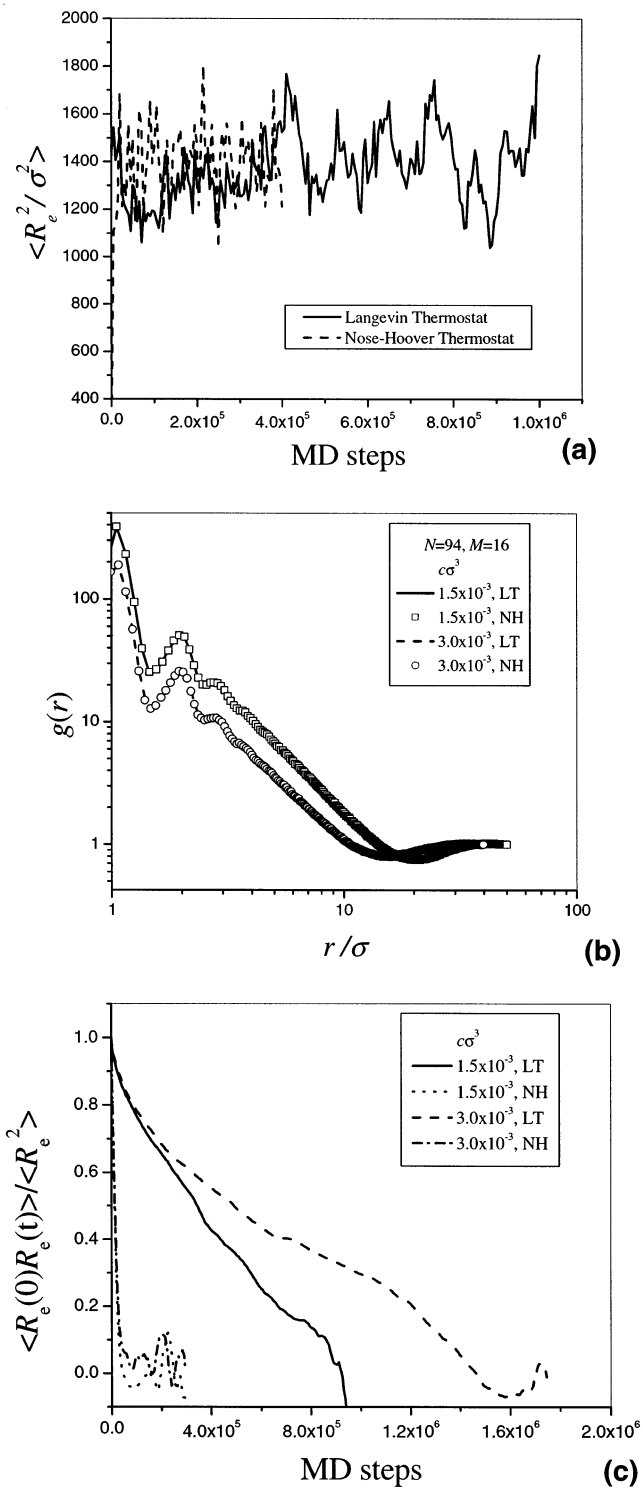

Figure 1. (a) Evolution of the root-mean-square end-to-end distances during simulation run for strongly charged chains with $f = 1$ and $N = 94$. Langevin thermostat (solid line) and Nose-Hoover thermostat (dashed line). (b) Monomer−monomer pair distribution function for strongly charged chains with $f = 1$ and $N = 94$. Abbreviations in the figure legend: Langevin thermostat (LT) and Nose-Hoover thermostat (NH). (c) Time correlation function of the end-to-end vector for strongly charged chains with $f = 1$ and $N = 94$. Abbreviations in the figure legend: Langevin thermostat (LT) and Nose-Hoover thermostat (NH).

3. Results and Discussion

3.1. Dilute Solutions. a. Nonuniform Stretching of Polyelectrolyte Chains. The intrachain electrostatic interactions dominate over the interchain ones in dilute solutions. To separate different length scales involved in the problem, it is useful to introduce the concept of electrostatic blob.[2,35−37] The nonuniform

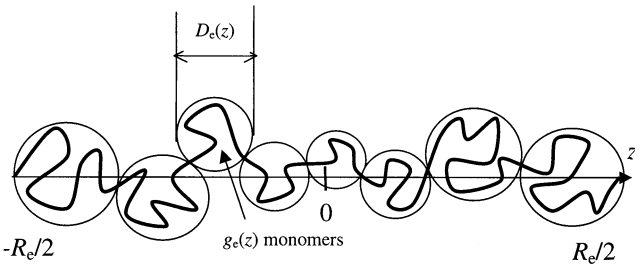

Figure 2. Schematic sketch of a polyelectrolyte chain in a dilute salt-free solution.

stretching of a polyelectrolyte chain[2,23] can be included by assuming that the blob size, $D_e(z)$, as well as the number of monomers in it, $g_e(z)$, depends on the position z along the direction of chain stretching (see Figure 2). The conformations of the chain inside the electrostatic blob are almost unperturbed by the electrostatic interactions. For a Θ-solvent for uncharged polymer backbone the relation between the blob size and the number of monomers in it is expected to be $D_e \approx b\sqrt{g_e}$, where b is the Kuhn length of the order of σ for our flexible polymers. For a single chain at extreme dilution we can neglect the effect of counterions. The reduced electrostatic potential at average position z along a single isolated chain is defined as $\varphi(z) = e\psi(z)/(k_BT)$, where $\psi(z)$ is the electrostatic potential at position z. The reduced electrostatic potential can be estimated by assuming one-dimensional charge distribution.

$$\varphi(z) \approx l_B\left(\int_{-R_e/2}^{z-D_e(z)/2} \frac{fg_e(y)}{D_e(y)}\frac{dy}{z-y} + \int_{z+D_e(z)/2}^{R_e/2} \frac{fg_e(y)}{D_e(y)}\frac{dy}{y-z} + \frac{fg_e(z)}{D_e(z)}\right) \quad (8)$$

Here, f is the fraction of charged monomers on the chain, R_e is chain size along the direction of elongation, and the center of the chain is located at $z = 0$. Assuming that the blob size $D_e(z)$ varies weakly with z and taking into account the relation between the number of monomers $g_e(z)$ in an electrostatic blob and its size $D_e(z)$, we can simplify expression 8

$$\varphi(z) \approx \frac{ufD_e(z)}{b}\left(\ln\left[\frac{R_e^2 - 4z^2}{D_e(z)^2}\right] + 1\right) \quad (9)$$

where u is the ratio of the Bjerrum length l_B to the bond size b. Equation 9 is valid in the interval from $-R_e/2 + D_e^0/2$ to $R_e/2 - D_e^0/2$, where $D_e^0 \approx b(uf^2)^{-1/3}$ is the size of the electrostatic blobs at chain ends. We can self-consistently find the electrostatic blob size using the classical path approximation for a strongly stretched chain. The force balance along the z-direction for a continuous chain model with the position of a monomer along the deformation direction z represented by $z(n)$, where n is the curvilinear coordinate along the chain contour, is

$$\frac{3}{b^2}\frac{d^2z(n)}{dn^2} \approx f\frac{d\varphi(z)}{dz} \quad (10)$$

The term on the left-hand side of eq 10 describes the elastic force acting on the nth monomer, balanced by the electrostatic force on the right-hand side of the equation. This equation is valid at any point along the chain except at chain ends where the tension $v(n) = dz(n)/dn$ vanishes ($v(0) = v(N) = 0$). The position of a monomer along the chain can be uniquely described within the strong stretching approximation by its projection on the deformation direction z. In this case the derivative d/dn can be transformed into the derivative with respect to z ($d/dn = v(z)\, d/dz$). Defining the local tension $v(z)$ in terms of the number of monomers $g_e(z)$ in the electrostatic blob and its size $D_e(z)$ ($v(z) = D_e(z)/g_e(z)$), one can rewrite eq 10 for the electrostatic blob size

$$\frac{3b^2}{2}\frac{d}{dz}D_e(z)^{-2} \approx f\frac{d\varphi(z)}{dz} \quad (11)$$

The solution of this equation with the electrostatic potential $\varphi(z)$ given by eq 9 can be approximated by

$$D_e(z) \approx D_e^0\left[\ln\left(\frac{R_e^2 - 4z^2}{2R_eD_e^0}\right) + 1\right]^{-1/3} \quad (12)$$

Thus, the smallest electrostatic blob is in the middle of the chain. This result is not surprising since the center of the chain experiences stronger electrostatic repulsion than chain sections closer to chain ends. The chain size is obtained from the monomers' conservation condition

$$N = 2\int_0^{R_e/2-D_e^0/2} \frac{g_e(z)\, dz}{D_e(z)} \approx \frac{R_eD_e^0}{b^2}\left(\ln\frac{eR_e}{D_e^0}\right)^{-1/3} \quad (13a)$$

The logarithmic term on the right-hand side of eq 13a accounts for the nonlinear stretching of the polyelectrolyte chain. Similar results for the chain size can be obtained using simple Flory-like arguments by balancing electrostatic and elastic energies of a polyelectrolyte chain.[2] An iterative solution of eq 13a yields the following expression for the chain size:

$$R_e \approx bNu^{1/3}f^{2/3}[\ln(N/g_e)]^{1/3} \quad (13b)$$

However, eq 13b is only valid in the range of parameters for which the chain size R_e is smaller than the size of fully stretched chain bN. This requirement leads to the upper bound on the chain degree of polymerization $N < u^{-2/3}f^{-4/3}\exp(u^{-1/3}f^{-2/3})$.

b. Monomer Density Distribution and Electrostatic Blob Size. In Figure 3a–c we compare the projection of the monomer density on to the direction of the end-to-end vector with the predictions of the scaling theory (eq 12)

$$\rho(z) = \frac{g_e(z)}{D_e(z)} \approx \frac{D_e(z)}{b^2} \approx \rho_0[\ln(R_e^2/4 - z^2) + B]^{-1/3} \quad (14)$$

where ρ_0 and B are adjustable parameters. These figures show an increase of monomer density with distance z from the chain center. The agreement between the modified scaling model and simulations is superb in the middle of the chain where the density fluctuations are small. However, fitting curves deviate from the simulation curves close to the chain ends. This discrepancy with the model predictions is not surprising since we used the strong stretching approximation that breaks down near the chain ends where chain tension decreases. The thickness of this fluctuating region near

Table 2. Electrostatic Blob Size D_e Used in Figure 4b

	$c = 5.0 \times 10^{-3}\sigma^{-3}$	$c = 1.5 \times 10^{-3}\sigma^{-3}$	$c = 5.0 \times 10^{-4}\sigma^{-3}$	$c = 1.5 \times 10^{-4}\sigma^{-3}$	$c = 1.5 \times 10^{-5}\sigma^{-3}$
$N = 25$	4.50	4.24	4.18	3.64	
$N = 40$	4.57	4.14	3.80	3.66	3.29
$N = 60$	4.84	4.20	4.02	3.70	3.35
$N = 94$		4.59	4.11	3.94	3.39
$N = 187$				3.63	3.30
$N = 300$					3.33

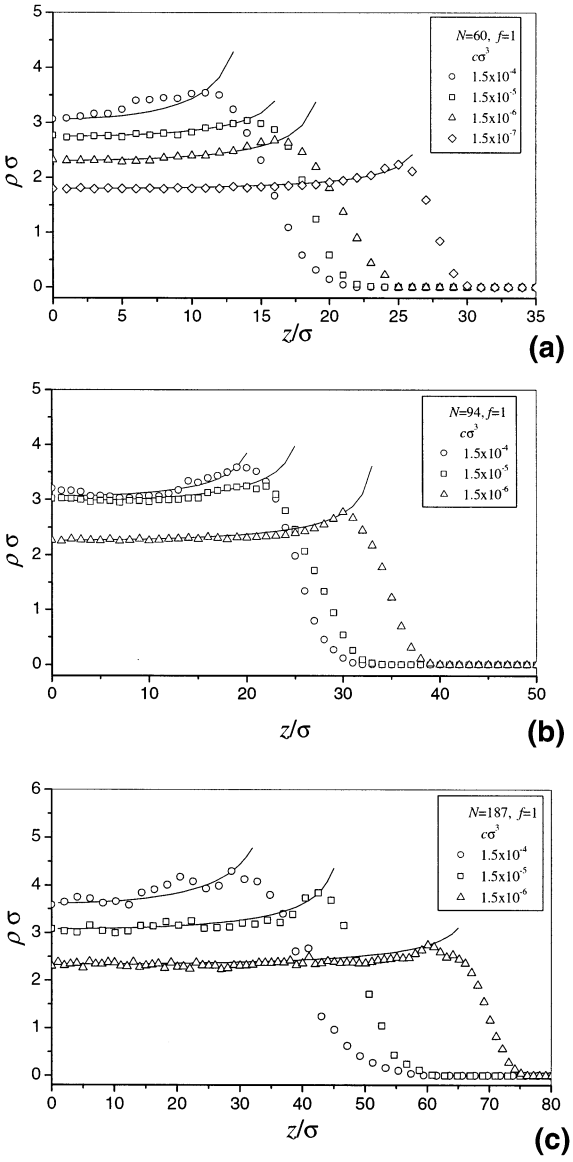

Figure 3. Projection of linear monomer density on the direction of the end-to-end vector for chains with $N = 60$ (a), $N = 94$ (b), and $N = 187$ (c). The symbols are results of MD simulations of strongly charged chains ($f = 1$), and the lines are best fits to eq 14.

chain ends is of the order of the Gaussian chain size $b\sqrt{N}$ because this is a typical length scale of the chain size fluctuations.

The linear monomer density $\rho(z)$ is proportional to the blob size $D_e(z)$ (see eq 14), and this set of plots (Figure 3) also shows the variation of the electrostatic blob size $D_e(z)$ along the direction of chain stretching. The variation in the electrostatic blob size between the middle and the ends of the chain becomes less pronounced as polymer concentration increases. This can be explained by the effective reduction of the charge on the chain due to counterion condensation. The effective charge on the chain, rather than the bare charge, determines the chain conformation. This effect can be included into the model of nonuniform chain stretching by substituting into eqs 8−13 f_e instead of a bare f value.

Another way of estimating electrostatic blob size is by comparing the difference in the elastic energy of the chain section containing g_e monomers with and without charges to the thermal energy k_BT. This method produces the variation of the electrostatic blob size with the monomer index along the chain (instead of the distance along the end-to-end vector). The elastic energy per bond of the uncharged chain includes contributions from both the LJ and FENE potentials and is equal to a constant $U_{e0} = 4.63k_BT$ independent of the chain length. For charged chains the electrostatic interactions between all charges in a system cause additional deformation of chain bonds. The conformations of chain sections become strongly influenced by these electrostatic interactions when the deformation energy exceeds thermal energy k_BT. Thus, comparing deformation energy $(U_e(k) - U_{e0})$ at the kth bond with the thermal energy k_BT, we can estimate the number of monomers $g_e(k) \sim k_BT/(U_e(k) - U_{e0})$ in the electrostatic blob. For example, the typical energy of the deformed bond for the chain with $N = 187$ at polymer concentration $c = 1.5 \times 10^{-4}\sigma^{-3}$ is $U_e \approx 4.96k_BT$. This leads to a typical number of monomers in the electrostatic blob $g_e \approx 3$ and a typical electrostatic blob size $D_e \approx 1.6\sigma$. The electrostatic blob size $D_e \approx 4\sigma$ estimated from the monomer density function (see Figure 3c) is about 2.3 times larger than the blob size estimated from the difference in the bond energies. The difference between blob sizes is due to the arbitrary choice of the bound of the bond deformation energy determining the blob size. We can improve the agreement between the two methods by setting this value to $2k_BT$ or even to $3k_BT$. In any case, both methods give comparable values of the electrostatic blob size up to a prefactor.

c. Chain Size. Figure 4 shows the end-to-end distance at various chain lengths and concentrations in dilute solution for fully charged chains ($f = 1$). We compare the data with scaling predictions given by eq 13a by constructing a universal plot using the value of the electrostatic blob size D_e obtained from linear monomer density distribution $\rho(z)$ averaged along the chain elongation direction. The plot of $R_eD_e(\ln eR_e/D_e))^{-1/3}$ as a function of N is shown in Figure 4b. Constructing this plot, we use the average blob size D_e (see Table 2) instead of D_e^0 in eq 13a. All data collapse on a universal curve that for longer chains approaches a straight line with unit slope. This is direct evidence of the nonuniform chain stretching and the applicability of the strong stretching approximation. The deviation from a straight line for short chains is due to the finite size effect. The fluctuations of the end-to-end distance for short chains are comparable with the average size of these chains. These fluctuations can be estimated from Figure 3. For chains with $N = 187$

monomers, the fluctuations in chain size $\sqrt{\langle \delta R_e^2 \rangle} \approx 10\sigma$ are about 10% of average chain size whereas for chains with $N = 40$, the fluctuations $\sqrt{\langle \delta R_e^2 \rangle} \approx 4\sigma$ are about 25%. In both cases fluctuations are of the order of $\sigma\sqrt{N}$ for these chains, which is about 14σ for $N = 187$ and 6σ for $N = 40$.

d. Intrachain Correlation Function. Additional information about chain structure can be obtained by analyzing the intrachain monomer−monomer correlation function that is proportional to the probability of finding a pair of monomers on the same chain separated by the distance r

$$g_{\text{intra}}(r) = \frac{1}{cN} \sum_{i \neq j} \langle \delta(\vec{r} - \vec{r}_{ij}) \rangle \qquad (15)$$

where brackets $\langle\ \rangle$ correspond to an ensemble average over all chain conformations and $\vec{r}_{ij}$ is the vector between ith and jth monomers on the chain. The summation in eq 15 is carried out over all pairs of monomers on the chain. In the strong stretching limit the fluctuations of the linear monomer density $\delta\rho(z)$ along the chain stretching direction z can be neglected in comparison with the average linear monomer density $\rho(z)$. In this case eq 15 can be written in terms of the average linear monomer density $\rho(z)$

$$g_{\text{intra}}(r) = \frac{1}{cN} \int_{-R_e/2}^{R_e/2} dz \int_{-R_e/2}^{R_e/2} dz'\, \rho(z)\, \rho(z') \langle \delta(\vec{r} - (z' - z)\vec{e}) \rangle_{\text{orient}} = \frac{1}{2\pi c N r^2} \int_{-R_e/2}^{R_e/2} dz\, \rho(z)\, \rho(z + r) \qquad (16)$$

where $\vec{e}$ is a unit vector along the chain elongation direction and brackets $\langle\ \rangle_{\text{orient}}$ denote averaging over all orientations of the unit vector $\vec{e}$. In the case of uniformly stretched chain with the average linear monomer density $\rho(z) = N/R_e$, eq 16 can be further simplified

$$g_{\text{intra}}(r) = \frac{N}{2\pi c r^2} \frac{R_e - r}{R_e^2} \theta(R_e - r) \qquad (17)$$

where $\theta(x)$ is the step function ($\theta(x) = 1$ for $x \geq 0$ and $\theta(x) = 0$ for $x < 0$). The intrachain pair correlation function $g_{\text{intra}}(r)$ follows a simple scaling law r^{-2} for distances $r \ll R_e$. In the case of nonuniformly stretched polyelectrolyte chain the average linear monomer density $\rho(z)$ varies logarithmically along the elongation axis (see eq 14). The intrachain correlation function $g_{\text{intra}}(r)$ counts the number of monomer pairs separated by the distance r. The summation over all monomer pairs leads to additional averaging of the linear monomer density $\rho(z)$ along the chain deformation direction. Both the end and the middle chain sections contribute to the function $g_{\text{intra}}(r)$ (see eq 16). Because of such averaging of the logarithmic function, one can expect the intrachain correlation function $g_{\text{intra}}(r)$ to be close to that for uniformly stretched chains (see Figure 5c). Figure 5 shows $cg_{\text{intra}}(r)$ for fully charged ($f = 1$) polyelectrolyte chains with degree of polymerization $N = 40$ (Figure 5a) and $N = 187$ (Figure 5b) in dilute solutions. At the intermediate length scales $r = 3\sigma - 6\sigma$ the slopes of the curves are close to -2.0 ± 0.05 for all five polyelectrolyte concentrations, in good agreement with theoretical predictions (see eq 17). For comparison, we fit the simulation result of $cg_{\text{intra}}(r)$ using the analytical form (eq 17) obtained for the stepwise monomer density distribution as well as by direct numerical integration (eq 16) of the linear monomer density $\rho(z)$ given in Figure 3. The results for the fully charged chains ($f = 1$) with the number of monomers $N = 187$ at polymer concentration $c = 1.5 \times 10^{-5}\sigma^{-3}$ are shown in Figure 5c. One can see that agreement between simulation data and both analytical results is excellent. In addition, it demonstrates that nonuniform chain stretching is not very important for the intrachain correlation function. A good approximation of this correlation function can be obtained from the uniform density profile.

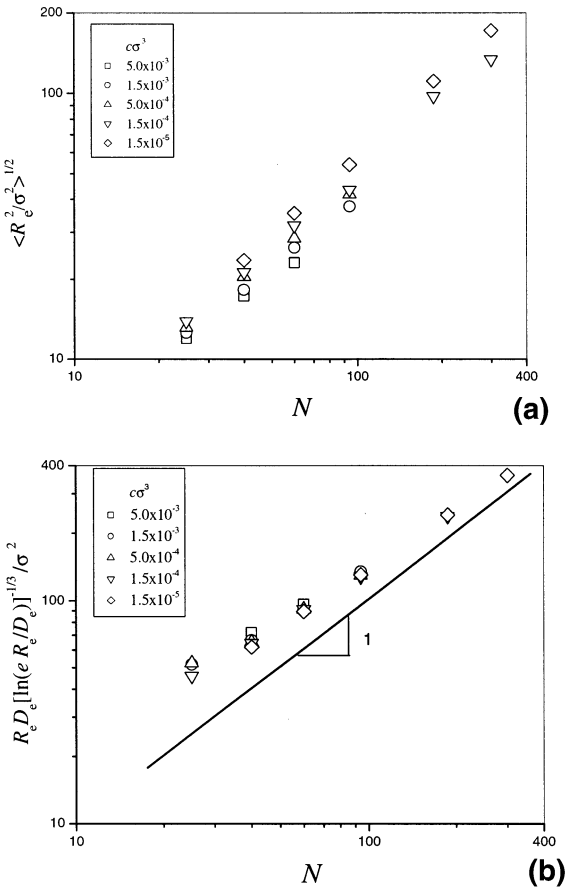

Figure 4. (a) Root-mean-square of end-to-end distance for various chain lengths and $f = 1$ in dilute solutions. (b) Universal plot of root-mean-square end-to-end distances obtained using eq 13 approaches solid line with slope 1 for longest chains.

e. Chain Contraction and Overlap Concentration. Polyelectrolyte chains begin to overlap when the distance between them becomes of the order of their size. Figure 6 illustrates the procedure for the estimation of the overlap concentration by the comparison of the concentration dependence of the distance between centers of mass of chains (thick solid line) and of the end-to-end distance (thin solid line) for chains with degree of polymerization $N = 94$. The two lines intersect at polymer concentration $c = (1.9 \pm 0.2) \times 10^{-3}\sigma^{-3}$, which we define to be the overlap concentration c^* for these chains. Note that the chain size is not constant below overlap concentration (see Figure 6), and the chain contracts significantly due to screening by counterions, which was not considered in the simple scaling

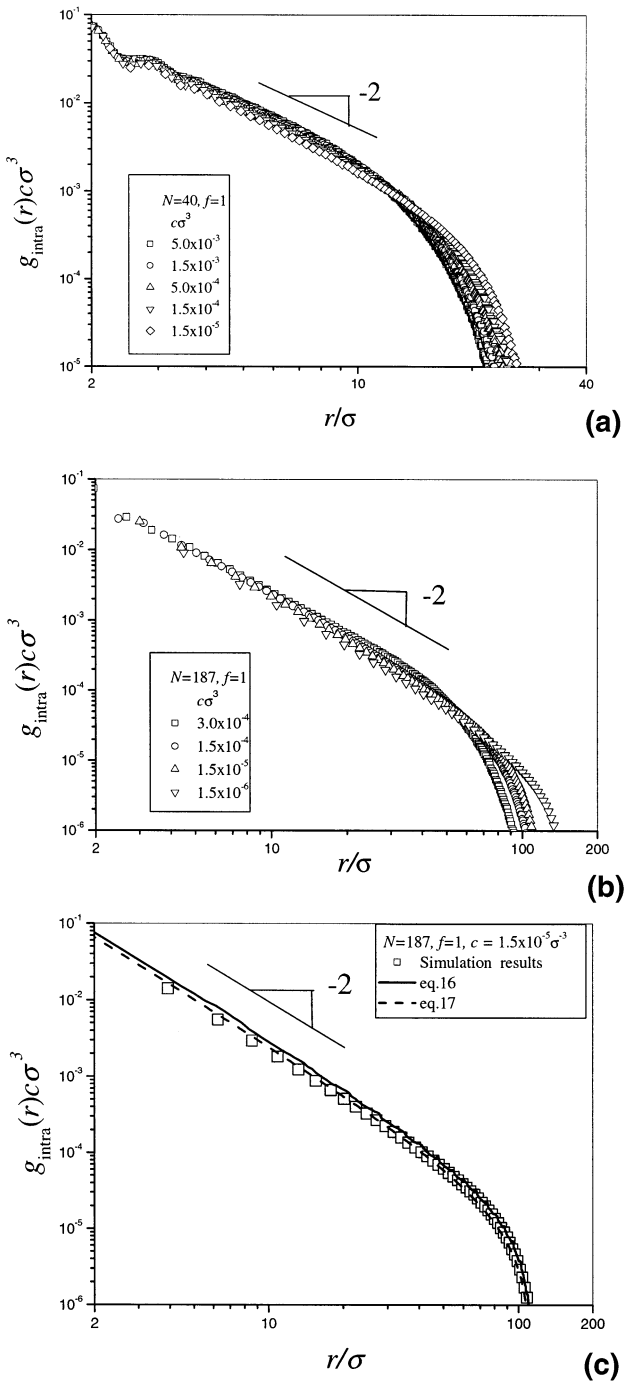

Figure 5. Intrachain monomer−monomer correlation function in dilute solutions for $f = 1$ and $N = 40$ (a) and $N = 187$ (b). The slopes are -2.0 ± 0.05 in the range $r = 3-6\sigma$ for all concentrations. (c) Comparison of the simulation results with predictions of eqs 16 and 17 (see text for details).

theory.[2,35−37] To illustrate this phenomenon further, Figure 7 shows dependence of the chain size on polymer concentration for different chain lengths and different values of charge parameter *f*. The corresponding overlap concentrations *c** for chains with a different number of monomers *N* are marked by arrows. All these curves show contraction of chain sizes with increasing polymer concentration. As one can see from Figure 7c,d, chains contract with almost the same rate; however, shorter chains reach saturation faster at higher concentrations.

For nonuniformly stretched chains, the relation between the number of monomers *N* and chain size R_e is

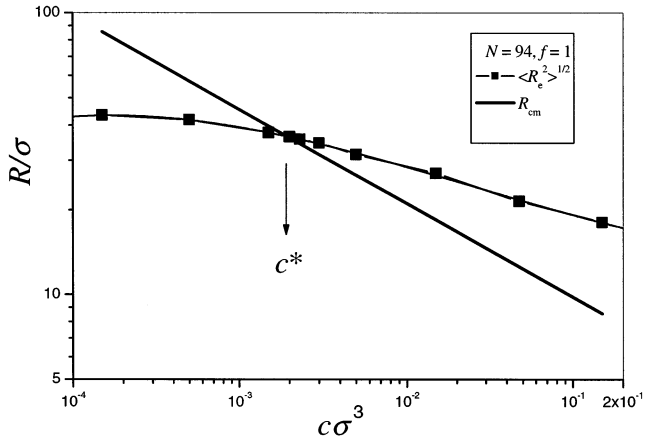

Figure 6. Concentration dependence of the chain size R_e and the distance between centers of mass of chains R_{cm} for polymers with $N = 94$ and $f = 1$. The overlap concentration is defined by $R_e = R_{cm}$.

given by eq 13a. Thus, the overlap concentration *c** can be estimated as

$$c^* \approx \frac{N}{R_e^3} \propto \frac{\ln^{-1/3}(R_e/D_e)}{R_e^2 b} \propto N^{-2}\ln^{-1}(N/g_e) \quad (18)$$

To verify this modified scaling prediction, we plot the dependence of the overlap concentration *c** on the chain degree of polymerization *N* for partially $f = {}^1/_3$ (circles) and fully $f = 1$ (squares) charged chains in Figure 8a. The solid and dashed lines correspond to eq 18. The dependence of the overlap concentration *c** on the chain degree of polymerization *N* seems to follow the scaling predictions eq 18 for the longer chains but deviates from it for shorter ones. This deviation from the scaling law can be attributed to the finite size effect. Short chains are not stretched enough to allow use of the strong stretching approximation in evaluation of their sizes. It follows from Figure 8a that the simulation curves for both charge densities $f = 1$ and $f = {}^1/_3$ have similar shapes. In Figure 8b we collapsed our simulation results into one universal curve. The numerical factor for this transformation is equal to 0.4. According to the scaling theory, this factor should be inversely proportional to the square of the ratio of the effective charge densities on the chains. For weakly charged chains with bare charge density $f = {}^1/_3$, this conversion factor is 0.11. This discrepancy between 0.11 and 0.4 can be explained by counterion condensation. The ratio of effective charge fractions on the two chains obtained from the osmotic coefficient is 0.69 (see ref 38), which is close to the expected value $\sqrt{0.4} \approx 0.63$. Thus, effective charge densities rather than the bare ones must be used for evaluation of conversion factor.

3.2. Semidilute Solutions. a. Scaling Model. The important length scale above the overlap concentration, $c > c^*$, is the correlation length ξ the average mesh size of the semidilute polyelectrolyte solution. Because the charge on the section of the chain with g_ξ monomers within correlation length ξ is compensated by counterions, the average charge of the correlation volume ξ^3 is equal to zero. The interactions between correlation volumes can be ignored in the zero-order approximation, and the electrostatic blob size and stretching of a chain can be estimated by taking into account only electrostatic interactions within correlation volume ξ^3. In fact,

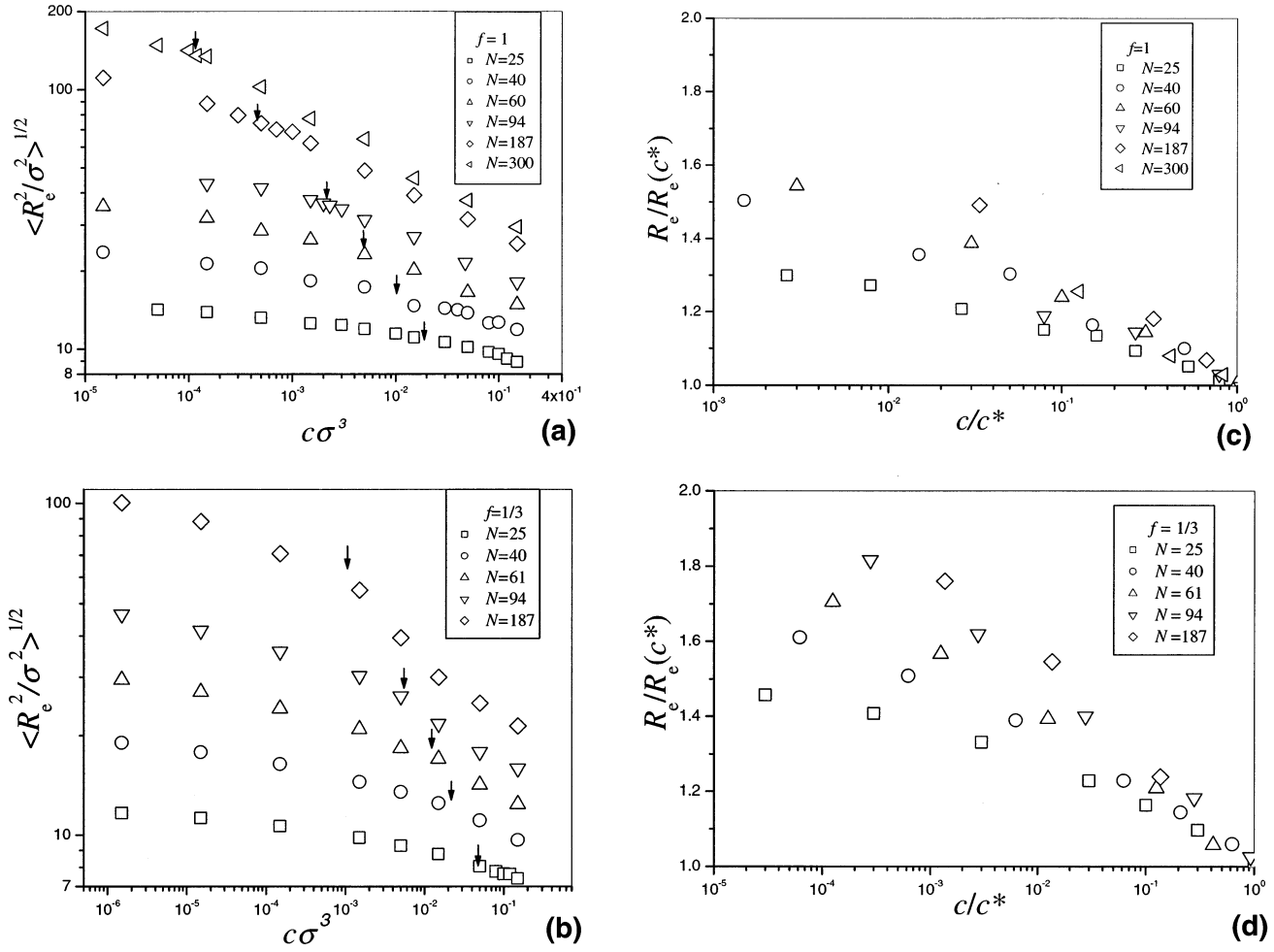

Figure 7. Concentration dependence of the chain size. (a) $f = 1$ and (b) $f = 1/3$. The overlap concentrations are marked by arrows. The normalized plots are shown in (c) for $f = 1$ and in (d) for $f = 1/3$.

the multipole expansion of electrostatic interactions between correlation volumes starts with quadrupole−quadrupole terms due to cylindrical symmetry inside the correlation volume. Thus, each charged monomer experiences electrostatic repulsion from all other charged monomers within the correlation volume and electrostatic attraction to the counterion background. This approximation corresponds to the well-known Katchalsky's cell model approximation.[7,39−41] Electrostatic interactions within correlation cell can be estimated by assuming that the cell has cylindrical symmetry with the polyelectrolyte chain located along the axis of the cylinder. The electrostatic interactions per monomer are

$$\frac{U_{el}}{k_B T} = 2 l_B f^2 \int_{D_e/2}^{\xi/2} \frac{g_e(z)}{D_e(z)} \frac{dz}{z} + \frac{l_B f^2 g_e}{D_e} - 2\pi l_B f \int_{-\xi/2}^{\xi/2} dz \int_0^{-\xi/2} \frac{c_{count}(r) r\, dr}{\sqrt{z^2 + r^2}} \quad (19)$$

where $c_{count}(r)$ is the counterion density profile. In eq 19, the first two terms describe the intrachain electrostatic interactions between a charged monomer and the chain section within correlation length ξ. The last term in this equation corresponds to attraction of the charged monomer to the counterion background. Since each monomer on the polyelectrolyte chain experiences the same electrostatic interactions, except for the monomers that are close to chain ends, we can assume that the chains are uniformly stretched such that $g_e(z)/D_e(z) =$ constant. In this case the two integrals over z in eq 19 can be evaluated easily. The last integral also can be evaluated if the counterion density profile around the polyelectrolyte chain is known. However, to obtain scaling relations between correlation length ξ and polymer concentration, one can assume a uniform density profile $c_{count}(r) = fc$. This leads to the following expression for the electrostatic interaction energy per monomer:

$$\frac{U_{el}}{k_B T} \approx \frac{l_B f^2 g_e}{D_e} \ln\left(\frac{\xi}{D_e}\right) - l_B f^2 c \xi^2 \quad (20)$$

The total interaction energy consists of the electrostatic part U_{el} and the elastic contribution due to stretching $k_B T D_e^2/(b^2 g_e)$ of a polyelectrolyte chain. Therefore, the interaction part of monomer chemical potential can be written as

$$\frac{\mu}{k_B T} \approx \frac{D_e^2}{b^2 g_e^2} + \frac{l_B f^2 g_e}{D_e} \ln\left(\frac{\xi}{D_e}\right) - l_B f^2 c \xi^2 \quad (21)$$

This expression has to be minimized with respect to the correlation length ξ and the electrostatic blob size D_e by taking into account the relation between the number of monomers in electrostatic blob g_e and its size ($D_e^2 \propto b^2 g_e$). This minimization leads to the following expres-

sion for the correlation length

$$\xi \ln^{1/6}\left(\frac{e\xi}{D_e^0}\right) \approx \left(\frac{D_e^0}{cb^2}\right)^{1/2} \quad (22)$$

and the blob size

$$D_e \approx D_e^0 \ln^{-1/3}\left(\frac{e\xi}{D_e^0}\right) \quad (23)$$

Thus, the correlation length (see eq 22) has only minor logarithmic correction to the well-known scaling form $\xi \propto c^{-1/2}$ (see refs 2 and 35−37)

$$\xi \propto c^{-1/2} \ln^{-1/6}\left(\frac{ec_e}{c}\right) \propto c^{-1/2} \quad (24)$$

The electrostatic blob size (eq 23) increases logarithmically with polymer concentration. The concentration dependence of the number of monomers in a correlation volume ξ can be obtained by imposing the close-packing condition for chain sections of size $\xi c \approx g_\xi/\xi^3$. This leads to the following concentration dependence of the number of monomers within a correlation length[2,35−37]

$$g_\xi \propto c\xi^3 \propto c^{-1/2} \ln^{-1/2}\left(\frac{e}{cD_e{}^0 b^2}\right) \approx c^{-1/2} \ln^{-1/2}\left(\frac{ec_e}{c}\right) \quad (25)$$

where c_e is the polymer concentration at which electrostatic blobs begin to overlap.

At the length scales larger than correlation length ξ, other chains and counterions screen electrostatic interactions, and the statistics of a chain is that of Gaussian chains with effective bond lengths of the order of the correlation length ξ. Thus, according to the scaling model, chain size R in the semidilute salt-free polyelectrolyte solution is a random walk of correlation blobs[2,35−37]

$$R \approx \xi\left(\frac{N}{g_\xi}\right)^{1/2} \propto N^{1/2}c^{-1/4} \ln^{1/12}\left(\frac{ec_e}{c}\right) \propto N^{1/2}c^{-1/4} \quad (26)$$

b. Correlation Length. The correlation length ξ in semidilute solutions can be estimated from the monomer−monomer pair correlation function $g(r)$ by comparing the interchain and intrachain contributions. The pair correlation function consists of intermolecular and intramolecular contributions

$$g(r) = g_{inter}(r) + g_{intra}(r) \quad (27)$$

The intramolecular correlation function was defined in eq 15. The intermolecular contribution to the pair correlation function is the sum over all pairs of molecules m and n (out of M chains in the system) and over all pairs of monomers on these molecules

$$g_{inter}(r) = \frac{1}{cMN} \left\langle \sum_{n\neq m=1}^{M} \sum_{i=1}^{N} \sum_{j=1}^{N} \delta(\vec{r} - \vec{r}_{ij}{}^{nm}) \right\rangle \quad (28)$$

where $\vec{r}_{ij}{}^{nm}$ is the vector between ith and jth monomers on the chains n and m, respectively. The pair correlation function $g(r)$ is proportional to the probability of finding a pair of monomers at distance r from each other. We define the correlation length ξ as the length scale at which these intra- and intermolecular contributions to the pair correlation function are equal. This means that at this distance ξ from a monomer on a given chain one can find with equal probability monomers belonging to the same or different chains. This method is designed to work in semidilute solutions. However, it fails in dilute solutions because the intrachain correlation function decays to zero exponentially fast at the length scales larger than the chain size where interchain contribution is still negligible. Figure 9 shows the pair correlation functions for chains with degree of polymerizations $N = 40$, 94, and 187 at monomer concentration $c = 0.015\sigma^{-3}$ as well as the interchain $g_{inter}(r)$ and intrachain $g_{intra}(r)$ contributions. The total monomer−monomer correlation function $g(r)$ is almost independent of the number of monomers on a chain N (see upper lines in Figure 9). However, both the intrachain and interchain correlation functions demonstrate some N dependence. The slope of the intrachain correlation function for chains with degree of polymerization $N = 40$ at intermediate length scales is -1.96 ± 0.02. This value is very close to the expected value -2 for strongly extended sections. For the shortest chains with $N = 40$, the concentration $c = 0.015\sigma^{-3}$ is very close to the overlap concentration $c^*_{N=40} = 0.01\sigma^{-3}$; thus, the conformation of these chains is almost rodlike. However, the conformation of the longer chains ($N = 94$ and 187) even at the length scales smaller than the correlation length is not rodlike. The slopes of intrachain correlation function at length scales $4.0\,\sigma < r < \xi$ are -1.63 ± 0.01

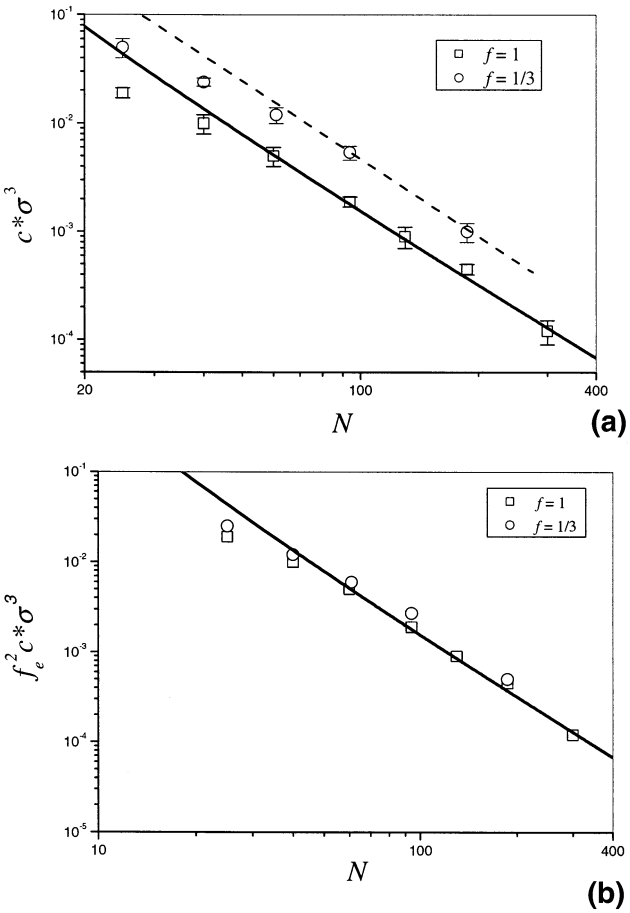

Figure 8. (a) Dependence of the overlap concentration on the number of monomers for partially $f = 1/3$ (circles) and fully $f = 1$ (squares) charged chains. Lines are predictions of eq 18. (b) Universal curve for the dependence of the overlap concentration on the number of monomers. The solid line is given by $c^* \sim N^{-2} \ln^{-1} N$.

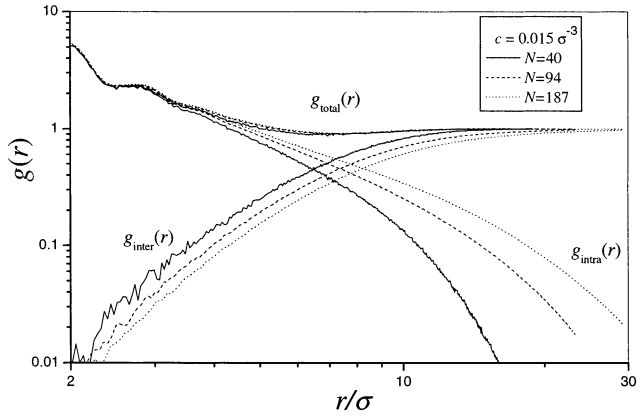

Figure 9. Monomer−monomer correlation function $g(r)$, intrachain monomer−monomer correlation function $g_{intra}(r)$, and interchain monomer−monomer correlation function $g_{inter}(r)$ for chains with $N = 40$ (solid line), 94 (dash line), and 187 (dot line) in semidilute solutions at polymer concentration $c = 0.015\sigma^{-3}$. The correlation length is estimated as the distance in which $g_{intra}(r) = g_{inter}(r)$. The slopes of the intrachain monomer−monomer correlation function $g_{intra}(r)$ within correlation blob ($4\sigma < r < \xi$) are -1.96 ± 0.02, -1.63 ± 0.01, and -1.46 ± 0.01 for $N = 40$, 94, and 187, respectively.

and -1.46 ± 0.01 for $N = 94$ and 187, respectively. This weak decay of the intrachain correlations may be an indication of the polyelectrolyte chain flexibility at the length scales r larger than the correlation length ξ (see discussion of the persistence length in semidilute solutions below).

Figure 10a summarizes data for concentration dependence of the correlation length ξ for several chain lengths. For the fixed chain length N, the slope of the correlation length approaches the scaling value $-1/2$ deep in the semidilute regime. However, for the same polymer concentrations, the correlation length increases with increasing the number of monomers N and, finally, saturates for longer chains. This saturation of the correlation length indicates that the N dependence of the correlation length is due to finite size effects. For shorter chains there are not enough correlation blobs per chain to completely suppress the contributions from chain ends. A plot of $\xi/R(c^*)$ as a function of c/c^* (Figure 10b) provides an estimate (with the logarithmic accuracy) of the number of blobs per chain. All our simulation data collapse onto one universal curve. The y-axis of this plot is inversely proportional (up to a logarithmic correction) to the number of correlation blobs per chain. The number of blobs per chain $R(c^*)/\xi$ in the semidilute solution increases with polymer concentration as $c^{1/2}$ as predicted by the scaling theory. It follows from this plot that for short chains the number of correlation blobs per chain does not exceed 10 throughout the entire semidilute regime. Finite size effects dominate chain properties of such short chains. However, for longer chains far from the overlap concentration, the number of blobs approaches 100, and finite size effects are suppressed.

c. Persistence Length and Chain Size. The scaling model of a polyelectrolyte chain in semidilute solutions is based on the assumption of the existence of a single length scale—the correlation length ξ. On length scales larger than the correlation length ξ, the conformations of a polyelectrolyte chain in semidilute solutions are assumed to be Gaussian. Thus, the polyelectrolyte chain is assumed to be flexible at length scales of the order of correlation length ξ. To check this scaling hypothesis,

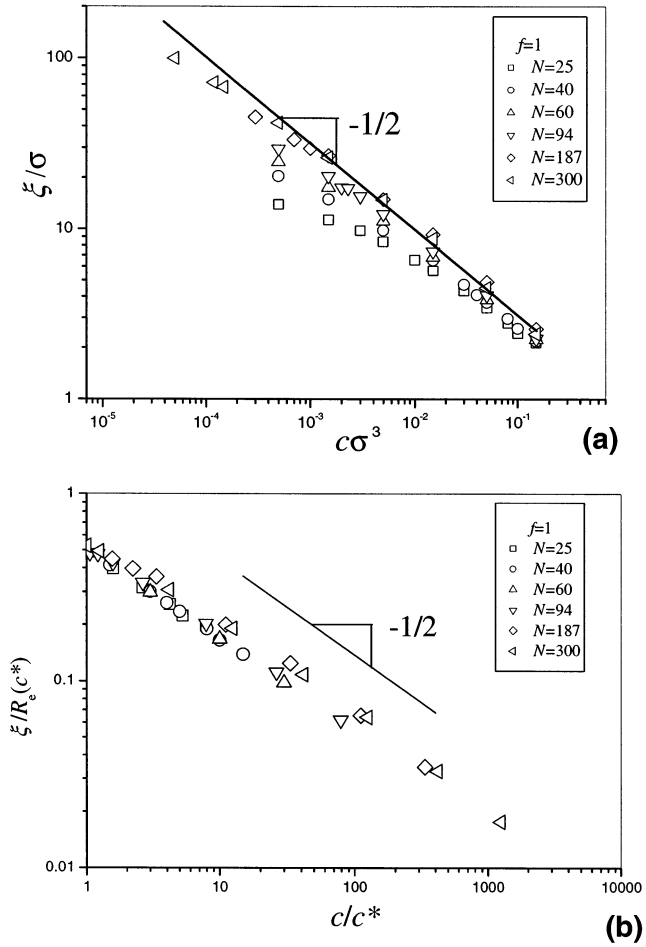

Figure 10. (a) Concentration dependence of the correlation length ξ. The line with slope $-1/2$ is shown to guide the eye. (b) $\xi/R_e(c^*)$ vs c/c^*. The line with slope $-1/2$ is shown to guide the eye.

we estimated the persistence length l_p in our simulations. The persistence length l_p (chain section containing k_p bonds) was calculated from the decay of the bond angle correlation function along the chain contour given by the following equation:

$$\langle \cos \phi_k \rangle = \frac{\vec{b}_s \cdot \vec{b}_{s+k}}{|\vec{b}_s||\vec{b}_{s+k}|} \propto \exp\left(-\frac{k}{k_p}\right)$$

Here, $\vec{b}_s$ and $\vec{b}_{s+k}$ are the bond vectors of sth and $(s+k)$ th bonds. We estimated the persistence length l_p as the square root of the mean-square end-to-end distance of a section of chain containing k_p bonds. The brackets $\langle\ \rangle$ denote the averaging over different chain conformations. We have performed averaging over different possible positions of s th bond vector along the chain ($s = 0, ..., N - k$), keeping the number of bonds k between the two vectors constant.

Figure 11 shows the bond angle correlation function of a fully charged ($f = 1$) polyelectrolyte chain with number of monomers $N = 300$ at different polymer concentrations in semidilute solutions. The bond angle correlation function has two regimes. At small distances within the electrostatic blob it decays very fast because the electrostatic interactions are too weak to orient the bonds. At the intermediate k values the decay is much slower due to the electrostatic interactions. The persistence length l_p in our simulations was estimated from the exponential decay of the bond angle correlation

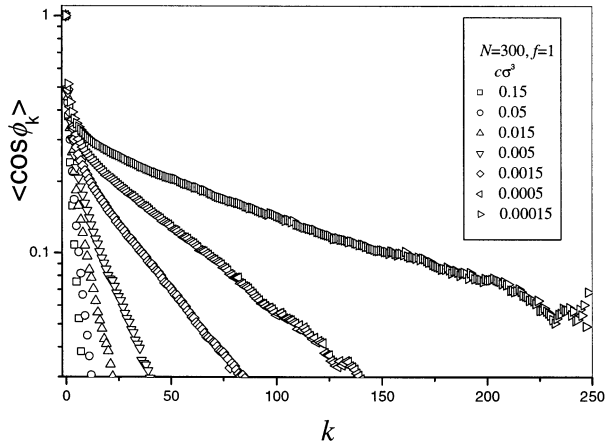

Figure 11. Dependence of the bond angle correlation function on the distance k along the chain for polymers with $N = 300$ and $f = 1$ at different polymer concentrations. Semilogarithmic scales.

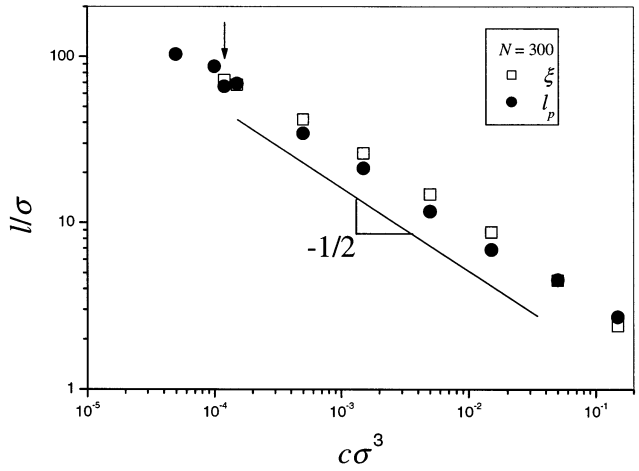

Figure 12. Concentration dependence of the persistence length l_p and correlation length ξ for chains with $N = 300$ and $f = 1$. The arrow marks the location of the overlap concentration.

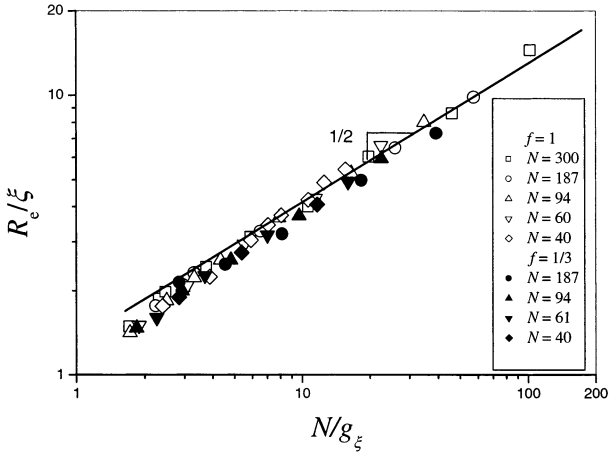

Figure 13. Dependence of the reduced chain size R_e/ξ on the number of correlation blobs N/g_ξ for chains with different degrees of polymerization, fraction of charged monomers, and at different polymer concentrations. Thin solid line has slope $^1/_2$.

function in the intermediate region.[26] Figure 12 shows our results for the concentration dependence of the electrostatic persistence length $l_p(c)$ and the correlation length $\xi(c)$ in semidilute polyelectrolyte solutions. As one

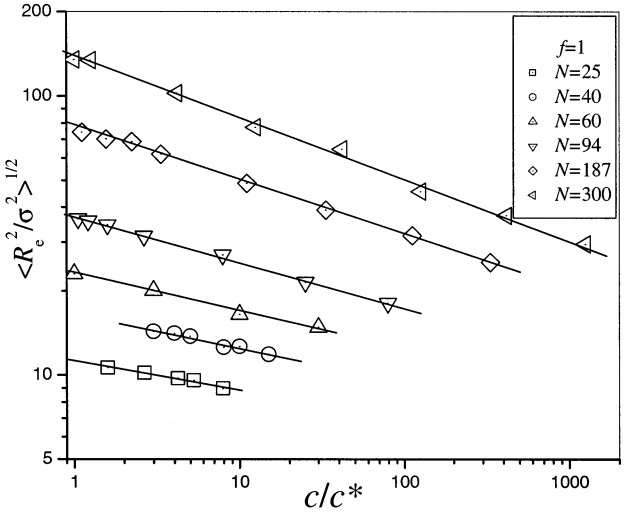

Figure 14. Dependence of the root-mean-square end-to-end distance for chains with $f = 1$ on reduced polymer concentration.

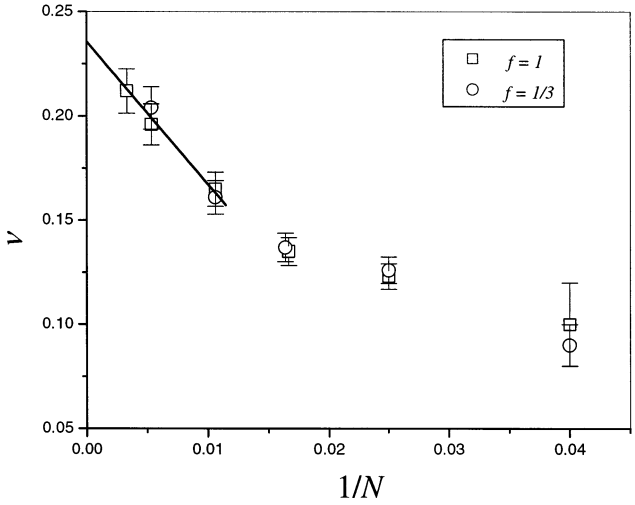

Figure 15. Variation of the scaling exponents for the root-mean-square end-to-end distance with the reciprocal number $1/N$ of monomers on a chain in semidilute solution. The line is the linear extrapolation of the exponents using the values for the three longest chain lengths.

can see from this plot, both length scales are proportional (in fact very close) to each other. These results support the hypothesis of single length scale in semidilute polyelectrolyte solutions in the range of degrees of polymerizations investigated in our simulations. Further confirmation of the scaling hypothesis[2,35,37] comes from the plot R_e/ξ vs N/g_ξ shown in Figure 13. All points for chains with different degrees of polymerization, different fractions of charged monomers, and at different polymer concentrations have collapsed into one universal line, with the slope $^1/_2$ as expected for Gaussian chains with N/g_ξ correlation blobs.

Figure 14 shows our data of the end-to-end distance for various chain lengths as a function of reduced concentration c/c^* in semidilute solutions. The results show that the concentration dependence of the chain size can be described by the power law $R \sim c^{-\nu}$; however, the exponent ν is N-dependent. We summarize the effective exponent ν of various chain lengths N in Figure 15. Our simulation results clearly show the transition from the weak concentration dependence of end-to-end distance of polyelectrolyte chain, $R_e \sim c^{-0.094}$ for

$N = 25$, to a stronger concentration dependence, $R_e \sim c^{-0.22}$ for $N = 300$. The concentration dependence of the chain size for the longest chains approaches the predicted value of the scaling exponent of $-1/4$.

4. Summary

We have performed molecular dynamics simulations of salt-free polyelectrolyte solutions composed of chains with number of monomers N from 25 to 300. Polyelectrolytes were modeled as charged Lennard-Jones particles connected to each other by the finite extension nonlinear elastic potential (eq 2). Counterions were included explicitly in our simulations. The electrostatic interactions between all charged species were taken into account by the smoothed particle mesh Ewald method.[31,32] Constant temperature ensemble simulations were performed by using Langevin and Nose-Hoover thermostats.

Our simulations show that the projection of the linear monomer density on the direction of chain elongation varies logarithmically along the elongation axis due to the nonuniform chain deformation in dilute solutions. The agreement between simulations and scaling predictions is excellent in the middle of the chain where the chain experiences strong stretching. However, the simulation data deviate from the scaling curves close to the chain ends where strong stretching approximation breaks down and fluctuations are important. The projection of the linear monomer density on the direction of chain elongation is proportional to the electrostatic blob size (see eq 14). Thus, polyelectrolyte chains can be represented by an array of electrostatic blobs, with size changing logarithmically along the direction of chain elongation and with the smallest blob located in the middle of the chain. Another consequence of the nonuniform stretching of polyelectrolyte chains is a logarithmic correction to the chain size dependence on the degree of polymerization. Using the average value of the electrostatic blob size, we were able to collapse all simulation data for the chain size dependence on the degree of polymerization for different polymer concentrations onto a single universal plot that approaches the scaling curve for the longest chains. However, the nonuniform stretching of polyelectrolyte chains in dilute solutions is not important for the intrachain monomer−monomer correlation function $g_{intra}(r)$. The intrachain correlation function $g_{intra}(r)$ counts the number of monomer pairs separated by the distance r. Both the end and the middle chain sections contribute to the function $g_{intra}(r)$ (see eq 16). Because of such averaging, the intrachain correlation function $g_{intra}(r)$ is well approximated by that of a rodlike chain with uniform linear monomer density (see Figure 5).

Crossover from a dilute to a semidilute regime occurs at polymer concentrations at which the distance between chains becomes comparable to the chain size. In our simulations we determined the overlap concentrations by comparing the root-mean-square end-to-end distance with the average distance between the centers of mass of neighboring chains. The simulation data for N dependence of polymer overlap concentration c^* approaches the scaling law $N^{-2} \ln^{-1} N$ as the degree of polymerization N increases (see Figure 8b).

Correlation length (correlation blob size) ξ is the important length scale, corresponding to the mesh size of a semidilute polyelectrolyte solution. The size of the correlation blob ξ in semidilute solutions can be obtained by the comparison of intra- and interchain contributions to the total monomer−monomer correlation function and is associated with a length scale where these two contributions are equal $g_{intra}(\xi) = g_{inter}(\xi)$. In semidilute solutions we found that the total correlation function is almost independent of the degree of polymerization N, while both intra- and interchain contributions show an N dependence. This N dependence of the inter- and intrachain correlation function as well as of the correlation length ξ is more pronounced for shorter chains but almost disappears for the set of our longest chains. Thus, such N dependence can be associated with the finite size effect. In the system of short chains the contribution of the chain ends is comparable to that from the middle of the chain, leading to a noticeable N dependence. For shorter chains as well as for longer ones close to overlap concentration there are about 3−8 correlation blobs per chain (see Figure 10b), which is not enough to eliminate the end effects. The exponent for concentration dependence of the correlation length is close to $-1/2$, predicted by the scaling model for all chain lengths.

The scaling model of polyelectrolyte chain in a semidilute solution assumes that the chain statistics at the length scales larger than correlation length ξ is a random walk of correlation blobs of size ξ. To test this assumption, we have evaluated the concentration dependence of the persistence length $l_p(c)$ from the bond angle correlation function. For our longest chains with $N = 300$, we found that the persistence length is proportional to the correlation length ξ (see Figure 12). Further evidence of chain flexibility comes from the plot of the reduced chain size R/ξ as a function of the number of correlation segments N/g_ξ (see Figure 13), which shows exponent $1/2$ predicted by the scaling model.[2,35,37] However, a word of caution should be said. The proportionality between persistence length and correlation length can be due to the fact that our chains are too short to observe the stiffening of polyelectrolyte chains caused by intrachain electrostatic interactions beyond the screening length that coincides with the correlation length ξ in semidilute solutions. Such stiffening of polyelectrolyte chains in semidilute polyelectrolyte solutions was predicted by Khokhlov and Khachaturian (KK),[42] who generalized the Odijk,[43] Skolnick,[44] and Fixman[44] (OSF) model of the electrostatic persistence length of a single polyelectrolyte chain with screened Debye−Huckel interactions. According to the KK model, the electrostatic persistence length l_p is proportional to the square of the screening length ($l_p \sim \xi^2/D_e$). Unfortunately, even in single-chain simulations the asymptotic OSF behavior of the persistence length was only observed for significantly longer polyelectrolyte chains with degrees of polymerization larger than $N = 2048$.[45−47] In simulations of shorter chains with $N = 256$ and 512 it was impossible to distinguish between linear and quadratic dependences of the persistence length l_p on the screening length.

According to the scaling model with $l_p \sim \xi$, a chain size R decreases with polymer concentration as $c^{-1/4}$. In our simulations the exponent for the concentration dependence of the chain size R is N-dependent (see Figure 15). It changes from the value -0.094 for the shortest chains with $N = 25$ to the value -0.22 for the longest ones ($N = 300$). This result for longest chains is very close to the prediction ($-1/4$) of the scaling model.[2,35,37]

Acknowledgment. The authors are grateful to the National Science Foundation for the financial support under Grant DMR-0102267 and to the donors of the Petroleum Research Fund, administered by the American Chemical Society, for the financial support under Grant 37018-AC7.

References and Notes

(1) Forster, S.; Schmidt, M. *Adv. Polym. Sci.* **1995**, *120*, 51.
(2) Barrat, J.-L.; Joanny, J.-F. *Adv. Chem. Phys.* **1996**, *94*, 1.
(3) Tanford, C. *Physical Chemistry of Macromolecules;* Wiley: New York, 1961.
(4) *Polyelectrolytes;* Hara, M., Ed.; Marcel Dekker: New York, 1993.
(5) Oosawa, F. *Polyelectrolytes;* Marcel Dekker: New York, 1971.
(6) Mandel, M. In *Encyclopedia of Polymer Science and Engineering*; Wiley: New York, 1988.
(7) Schmitz, K. S. *Macroions in Solution and Colloidal Suspension;* VCH: New York, 1993.
(8) *Physical Chemistry of Polyelectrolytes;* Radeva, T., Ed.; Marcel Dekker: New York, 2001.
(9) Flory, P. J. *Principles in Polymer Chemistry;* Cornell University Press: Ithaca, NY, 1953.
(10) deGennes, P.-G. *Scaling Concepts in Polymer Physics;* Cornell University Press: Ithaca, NY, 1979.
(11) Doi, M.; Edwards, S. F. *The Theory of Polymer Dynamics*; Oxford University Press: Oxford, 1986.
(12) Brender, C. *J. Chem. Phys.* **1990**, *92*, 4468.
(13) Brender, C. *J. Chem. Phys.* **1991**, *94*, 3213.
(14) Brender, C.; Danino, M. *J. Chem. Phys.* **1992**, *97*, 2119.
(15) Hooper, H. H.; Prausnitz, J. M. *Macromolecules* **1990**, *23*, 4820.
(16) Christos, G. A.; Carnie, S. L. *J. Chem. Phys.* **1989**, *91*, 439.
(17) Higgs, P. G.; Orland, H. *J. Chem. Phys.* **1991**, *95*, 4508.
(18) Barrat, J. L.; Boyer, D. *J. Phys. II* **1993**, *3*, 343.
(19) Ullner, M.; Jonsson, B.; Widmark, P. O. *J. Chem. Phys.* **1994**, *100*, 3365.
(20) Joensson, B.; Peterson, C.; Soederberg, B. *J. Phys. Chem.* **1995**, *99*, 1251.
(21) Peterson, C.; Sommelius, O.; Soederberg, B. *J. Chem. Phys.* **1996**, *105*, 5233.
(22) Migliorini, G.; Rostiashvili, V. G.; Vilgis, T. A. *Eur. Phys. J. E* **2001**, *4*, 475.
(23) Castelnovo, M.; Sens, P.; Joanny, J.-F. *Eur. Phys. J. E* **2000**, *1*, 115.
(24) Stevens, M.; Kremer, K. *Macromolecules* **1993**, *26*, 4717.
(25) Stevens, M.; Kremer, K. *Phys. Rev. Lett.* **1993**, *71*, 2228.
(26) Stevens, M.; Kremer, K. *J. Chem. Phys.* **1995**, *103*, 1669.
(27) Micka, U.; Holm, C.; Kremer, K. *Langmuir* **1999**, *15*, 4033.
(28) Micka, U.; Kremer, K. *Eur. Phys. Lett.* **2000**, *49*, 189.
(29) Chang, R.; Yethiraj, A. *J. Chem. Phys.* **2002**, *116*, 5284.
(30) Adams, D.; Dubey, G. *J. Comput. Phys.* **1987**, *72*, 156.
(31) Essman, U.; Perera, L.; Berkovitz, M. L. *J. Chem. Phys.* **1995**, *103*, 8577.
(32) Forester, T. R.; Smith, W. *The DL_POLY_2 Reference Manual*; Daresbury Laboratory: Daresbury, 2000.
(33) Turq, P.; Lantelme, F. *J. Chem. Phys.* **1977**, *66*, 3039.
(34) Hoover, W. G. *Phys. Rev. A* **1985**, *31*, 1695.
(35) deGennes, P.-G.; Pincus, P.; Velasco, R. M.; Brochard, F. *J. Phys. (Paris)* **1976**, *37*, 1461.
(36) Rubinstein M.; Colby, R. H.; Dobrynin, A. V. *Phys. Rev. Lett.* **1994**, *73*, 2776.
(37) Dobrynin, A. V.; Colby, R. H.; Rubinstein, M. *Macromolecules* **1995**, *28*, 1859.
(38) Liao, Q.; Dobrynin, A. V.; Rubinstein, M. *Macromolecules* **2003**, *36*, 3399.
(39) Fuoss, R. M.; Katchalsky, A.; Lifson, S. *Proc. Natl. Acad. Sci. U.S.A.* **1951**, *37*, 579.
(40) Alfrey, T., Jr.; Berg, T. W.; Morawetz, H. *J. Polym. Sci.* **1951**, *7*, 543.
(41) Katchalsky, A.; Alexandrowicz, Z.; Keden, O. In *Chemical Physics of Ionic Solutions*; Conway, B. E., Barradas, R. O., Eds.; Wiley: New York, 1966; p 266.
(42) Khokhlov, A. R.; Khachaturian, K. A. *Polymer* **1982**, *23*, 1742.
(43) Odijk, T. *J. Polym. Sci., Polym. Phys.* **1977**, *15*, 477.
(44) Skolnick, J.; Fixman, M. *J. Chem. Phys.* **1977**, *10*, 944.
(45) Ullner, M.; Woodward, C. E. *Macromolecules* **2002**, *35*, 1424.
(46) Everaers, R.; Milchev, A.; Yamakov, V. *Eur. Phys. J. E*, in press.
(47) Nguyen, T. T.; Shklovskii, B. cond-mat/0202168v2.

MA025995F